Clim Dyn (2015) 45:253–271
DOI 10.1007/s00382-014-2411-2

Interannual variability of autumn to spring seasonal precipitation in eastern China

Kairan Ying · Tianbao Zhao · Xiao-Wei Quan · Xiaogu Zheng · Carsten S. Frederiksen

Received: 7 March 2014 / Accepted: 11 November 2014 / Published online: 21 November 2014

Abstract The interannual variability of seasonal precipitation in eastern China from fall to following spring is examined for the period of 1951–2004 based on observations at 106 stations. The temporal variability of seasonal mean values is decomposed into intraseasonal (fast) and slow (potentially predictable) components. EOF analysis is then applied to both the fast and predictable components. We find that (1) the most predictable signal migrates in a north–south direction along with the annual cycle of the monsoon in east China, while spatial patterns of the leading fast modes does not change much; (2) the predictable signal of precipitation in eastern China is associated with anomalous atmospheric circulation patterns having more zonally symmetric structures while the fast time-varying precipitation components are accompanied by wavy anomalous atmospheric circulation patterns; (3) the most predictable signal has an apparent 1-season lagged correlation with the interannual variation of sea surface temperature associated with El Niño/Southern Oscillation; (4) The fast rainfall component is largely attributed to the intraseasonal variabilities of the Siberian High over the Eurasian continent and the subtropical high associated with the Western-Pacific-Oscillation-like variabilities over the North Pacific; and (5) The ENSO signal in the fall seasonal precipitation persisted throughout the entire 54-year period while the signal in winter intensified significantly after the mid-1970s. This is attributed to the weaker/stronger intensification of ENSO anomalies in the tropical Pacific during the fall/winter.

Keywords Rainfall · ENSO · Interdecadal change · Seasonal predictable · Intraseasonal · Siberian High · Subtropical high

1 Introduction

Climate variability related to seasonal precipitation in east China is an attractive research subject because of its importance to the agriculture and other societal needs in the most populated area in China (e.g. Ding 1994; Chang 2004; Wang 2006). Many previous studies have focused on the variability of the precipitation during the summer season (e.g. Ding and Chan 2005; Zhou et al. 2011; Hsu et al. 2014) and found that the behavior of summer precipitation in east China is determined by impacts of multiple forcing factors from the tropical Pacific at interannual (e.g. Huang and Sun 1994; Hu 1997; Chang et al. 2000; Wang and Li 2004; Wang et al. 2008a, 2009; Zhou et al. 2009a; Li and Zhou 2011; He et al. 2013) and interdecadal time-scales (e.g. Wang et al. 2008b; Zhou et al. 2008; Li et al. 2010a, b; Zhou et al. 2013; Qian and Zhou 2014), the tropical Indian Ocean (e.g. Yang et al. 2007; Wu et al. 2009; Zhou et al. 2009b; Li et al. 2010a, b), the western Pacific (e.g. Wu et al. 2010; Song and Zhou 2014), the North Atlantic

K. Ying · X. Zheng
College of Global Change and Earth System Science, Beijing Normal University, Beijing, China

K. Ying · T. Zhao
Key Laboratory of Regional Climate-Environment Research for East Asia, Institute of Atmospheric Physics, Chinese Academy of Sciences, Beijing, China

X.-W. Quan (✉)
Cooperative Institute for Research in Environmental Sciences, University of Colorado at Boulder and NOAA/ESRL/PSD, Boulder, CO, USA
e-mail: quan.xiao-wei@noaa.gov

C. S. Frederiksen
The Centre for Australian Weather and Climate Research, Bureau of Meteorology, Melbourne, Australia

(e.g. Linderholm et al. 2011; Zuo et al. 2013), and snow conditions over the Tibetan Plateau and the Eurasia continent (e.g. Wu and Qian 2003; Zhang et al. 2004; Wu and Kirtman 2007; Zhao et al. 2007, 2009b). It has also been found that intraseasonal variability is another important factor contributing to the behavior of seasonal precipitation in the region of East Asia Monsoon (e.g. Mao and Chan 2005).

As part of the East Asian Monsoon (EAM) system, it is also important to understand the variability of the seasonal precipitation in non-summer seasons. Some previous studies examined the variability of EAM for non-summer seasons in the context of understanding the connection between EAM and El Nino-Southern Oscillation (ENSO). Zhang et al. (1999) found that the spatial structure of ENSO impact in non-summer seasons has a different spatial structure than its counterpart in summer. Wu et al. (2003) indicated that during the developing phase of an ENSO event the impact of ENSO appears with two active centers—a positive one in south China being effective from fall through to the following spring; and a negative one in North China being effective from summer to fall. Wang et al. (2000) revealed that the interannual variability of precipitation in EAM is connected to ENSO via an anomalous lower-tropospheric anticyclone/cyclone over the western North Pacific that starts in late fall of the maturing year of ENSO and persists until the following spring. More recent studies further suggested that the interannual variability of EAM during the non-summer seasons have two major modes: one is associated with the decaying phase of ENSO and has prominent biennial tendency; the other evolves with the developing phase of ENSO (Wang et al. 2008a). While circulation and precipitation anomalies in the two modes behave differently, impacts of ENSO are important in both modes during the seasons of fall to the following spring (Wang et al. 2008b; Wu et al. 2009; Zhou et al. 2009a). The study by Wu et al. (2009) also suggested an involvement of air-sea interactions over the tropical Indian Ocean in the evolution of the second mode. In this study, the variability of precipitation in the eastern China for the seasons from fall to the following spring and its connections to remote SST forcing and tropical/extratropical atmospheric circulation anomalies are further examined to understand ENSO and non-ENSO related behaviors of the interannual variability in the autumn to spring rainfall in eastern China. Using the method of Zheng and Frederiksen (2004) that effectively partitions seasonally predictable (slow) component and intraseasonal (fast) component from covariance of seasonal mean time series (see Sect. 2 for explanation), we show that the identified slow component of the rainfall variability can be mostly explained by the ENSO related SST variability in the tropical Pacific, consistent with the results found by the previous authors. We also show that the intraseasonal components during this time of year mainly consists of two modes: one is also sensitive to the conditions of atmospheric circulation anomalies having ENSO alike spatial pattern in the tropics; another is more linked to anomalous conditions of the Siberian High that does not have apparent connections to tropical forcing.

It has been widely noticed that some apparent climate changes had happened in EAM around the mid-1970s (see the review by Zhou et al. 2009b and references there). One remarkable aspect of the changes is the connection between the interannual variability of EAM and ENSO. Changes has been found in the correlation between the anomalous SST conditions in the tropical eastern Pacific and the seasonal precipitation anomalies in east China, and other EAM activities for summer (Chang et al. 2000; Wu and Wang 2002), winter (Wang and He 2012), winter and spring (Chen et al. 2013). Whether the connection between EAM and ENSO had been strengthened or weakened is a topic of debating in some recent papers. For example the sdudy by Wang et al. (2008b) suggested that the overall coupling between the monsoon activities in Asian-Australian regions and ENSO has been strengthened since the late 1970s while the papers by Wang and He (2012), Chen et al. (2013) argued that the EAM-ENSO relation has been weakened. In the study of Ying et al. (2013) we found that for the seasons from late-fall to early-winter relationship between precipitation in the Yangtze River Valley and ENSO had been persistent throughout the 54-year period of 1951–2004 with no significant interdecadal changes, which may have been due to the limited area considered in that study. In this paper we attempt to better understand this earlier result by extending that analysis to the broader region of east China.

Data and method are described in Sect. 2; analyses of the interannual and intraseasonal variability of the late fall to winter seasonal precipitation in east China are presented in Sects. 3.1 and 3.3; circulation patterns associated with the predictable precipitation modes are discussed in Sect. 3.2; interdecadal changes in the correlation between the seasonal precipitation in east China and the tropical eastern Pacific SST are examined in Sect. 3.4; conclusions and discussions are presented in Sect. 4.

2 Data and method

2.1 Datasets

The monthly precipitation dataset used in this study is from a network of 106 stations in eastern China (Fig. 1) for the period from January 1951 to December 2004, provided by the China Meteorological Administration. For the purposes of this study, eastern China refers to the region of 20°–45°N and 110°–130°E, which is the region most influenced by the East Asian Monsoon (Wang and Linho 2002)

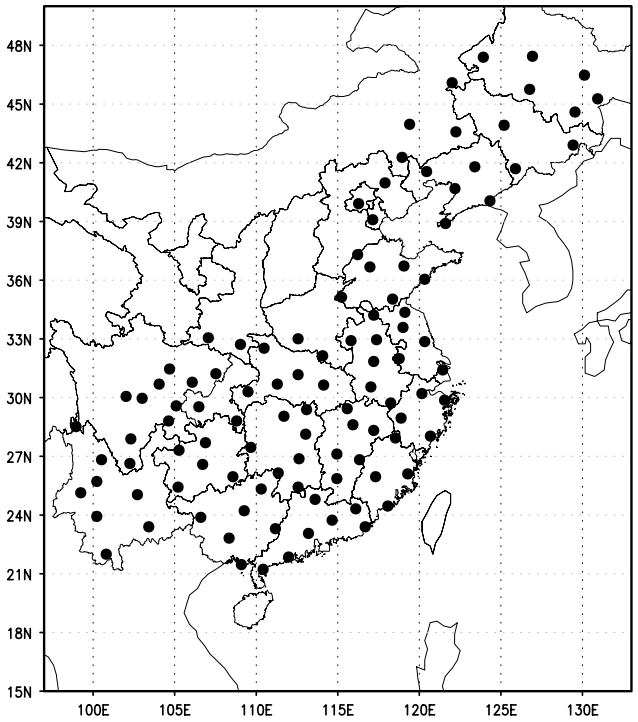

Fig. 1 The 106 stations of which monthly precipitation data are adopted in this study

and therefore readily lends itself to a physical explanation of the derived predictable modes. For global analyses, monthly precipitation data from the National Centers for Environmental Prediction-National Center for Atmospheric Research (NCEP-NCAR) reanalysis (Kalnay et al. 1996) with a horizontal resolution of approximately 1.9° × 1.9° were used. Monthly mean wind field and geopotential height at 500 hPa are derived from the NCEP-NCAR reanalysis for the period 1951–2004, which have a horizontal resolution of 2.5° × 2.5°. Monthly outgoing longwave radiation (OLR) data on a 2.5° × 2.5° latitude/longitude grid, obtained from National Oceanic and Atmospheric Administration (NOAA, Liebmann and Smith 1996), are used for the period 1974–2004. The monthly mean sea surface temperatures (SST) on a 1.0° × 1.0° grid is obtained from the UK Met Office Hadley Centre Sea Surface Temperature dataset (HADISST1.1; Rayner et al. 2003) for the same 54 year period.

2.2 Decomposition of covariability

Zheng and Frederiksen (2004) proposed a methodology for extracting, from monthly mean data, spatial patterns of interannual (supra-annual) variability in seasonal mean fields that can be related to variability of slow and intraseasonal components. Frederiksen and Zheng (2007) provide a review of the underlying ideas and applications of the general methodology. Readers are referred to the papers for a detailed description of the methodology. Here, we present only a brief summary of the method.

Firstly, the annual cycle is removed from the data. The monthly time series of each climate anomaly is then conceptually decomposed into two components consisting of a seasonal "population" mean and a residual departure from this mean. Thus, if x_{ym} represents sample monthly values, within a season, in month m (m = 1, 2, 3) in year y (y = 1, …, Y, where Y is the total number of years), we use the following decomposition (for example, ZF2004),

$$x_{ym} = \mu_y + \varepsilon_{ym}. \tag{1}$$

Here, μ_y is the seasonal population mean in year y, and ε_{ym} is a residual monthly departure of x_{ym} from μ_y and arises from intraseasonal variability. The vector $\{\varepsilon_{y1}, \varepsilon_{y2}, \varepsilon_{y3}\}$ is assumed to comprise a stationary and independent annual random vector with respect to year. Equation (1) implies that month-to-month fluctuations, or intraseasonal variability, arise entirely from $\{\varepsilon_{y1}, \varepsilon_{y2}, \varepsilon_{y3}\}$ (e.g. $(x_{y1} - x_{y2} = \varepsilon_{y1} - \varepsilon_{y2})$.)

We represent an average taken over an independent variable (i.e. m or y) by replacing that variable subscript with "o". For example, x_{yo} indicates the seasonal average of x_{ym} in year y and x_{oo}, the average of x_{ym} taken over all months and years. With this notation, a seasonal mean can be expressed as

$$x_{yo} = \mu_y + \varepsilon_{yo}, \tag{2}$$

where ε_{yo} is associated with intraseasonal variability and μ_y with the interannual variability of external forcing and slowly varying (interannual/supra-annual) internal dynamics. ZF2004 refer to these as the intraseasonal and "slow"or predictable component, respectively, of the seasonal meanx_{yo}, which is also referred to as the "total" component. Since dynamic prediction has a skillful range of about 10 days, the interannual variability arising from intraseasonal variability is not predictable at seasonal time scales. Therefore, we shall also refer to the intraseasonal component as the unpredictable component. In addition, we shall also refer to the slow component as the potentially predictable component.

Following Madden (1976), we define the *potential predictability* as the ratio between the variance of the predictable component ($V(\mu_y)$)and the variance of the total component ($V(x_{yo})$) (Zheng and Frederiksen 1999), which can be expressed as

$$p = \frac{V(\mu_y)}{V(x_{yo})}, \tag{3}$$

It represents the fraction remaining after the removal of the intraseasonal component from the total. The larger the potential predictability, the more likely the seasonal mean precipitation anomalies can be predicted.

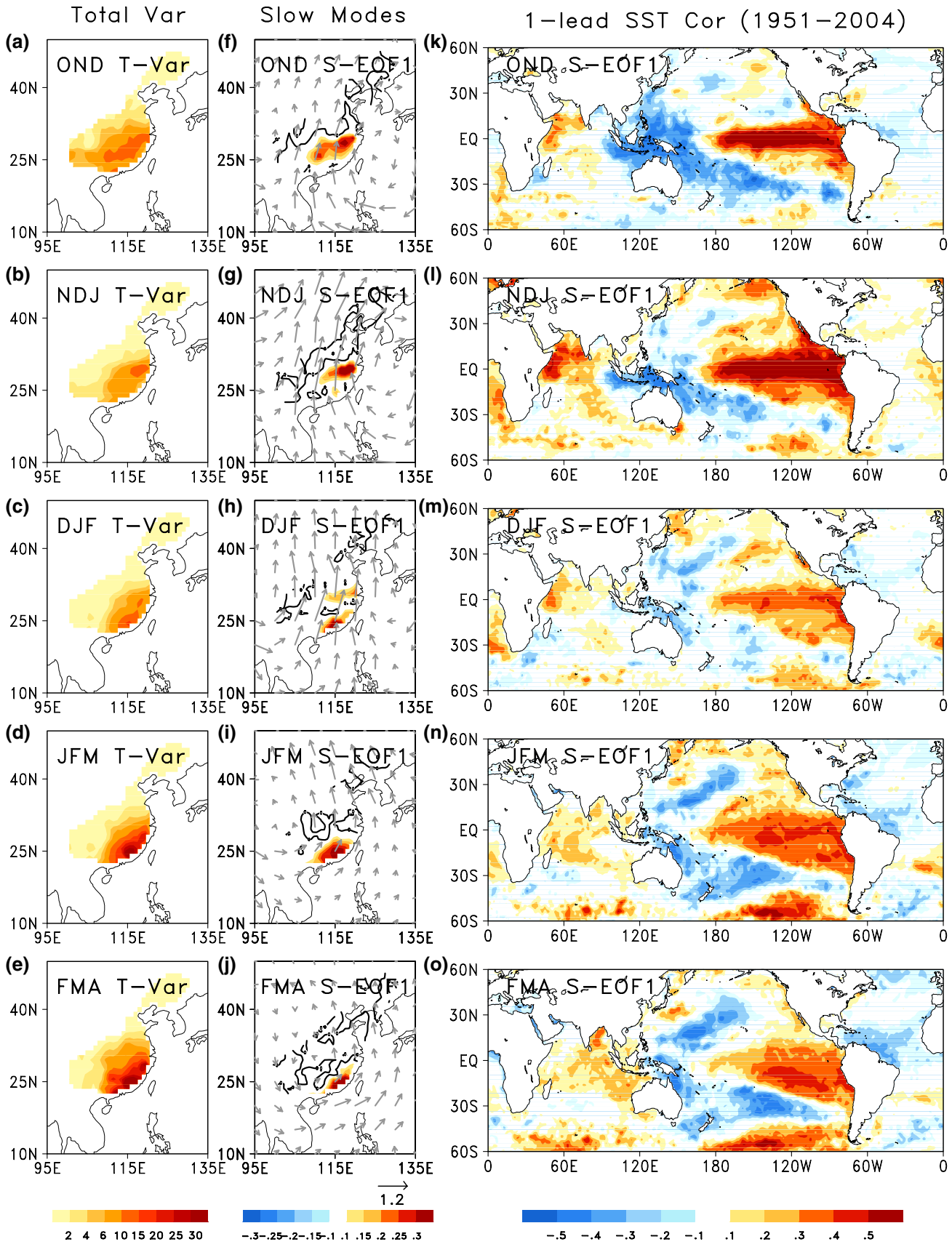
Total Var
Slow Modes
1−lead SST Cor (1951−2004)
(a) OND T−Var
(b) NDJ T−Var
(c) DJF T−Var
(d) JFM T−Var
(e) FMA T−Var
(f) OND S−EOF1
(g) NDJ S−EOF1
(h) DJF S−EOF1
(i) JFM S−EOF1
(j) FMA S−EOF1
(k) OND S−EOF1
(l) NDJ S−EOF1
(m) DJF S−EOF1
(n) JFM S−EOF1
(o) FMA S−EOF1
40N
25N
10N
95E
115E
135E
60N
30N
EQ
30S
60S
0
60E
120E
180
120W
60W
1.2
2 4 6 10 15 20 25 30
−.3 −.25 −.2 −.15 −.1 .1 .15 .2 .25 .3
−.5 −.4 −.3 −.2 −.1 .1 .2 .3 .4 .5

◂**Fig. 2** Spatial distribution of total variance (*left*; unit: 100 mm^2), leading slow mode and the covariance between the associated time series for the slow rainfall mode and the slow component of 500 hPa wind field (*center*), and the 1-season lag correlation between PC time series of the leading slow modes and SST (*right*) for the five consecutive 3 month periods from late-fall (OND) to early spring (FMA)

Suppose now that we have two climate variables x_{ym} and x'_{ym} that satisfy Eqs. (1) and (2). Then, ZF2004 derived the following estimate of the interannual covariance $V(\varepsilon_{yo}, \varepsilon'_{yo})$ of the intraseasonal components,

$$V(\varepsilon_{yo}, \varepsilon'_{yo}) \approx \hat{\sigma}^2(3 + 4\hat{\varphi})/9, \tag{4}$$

where,

$$\hat{\sigma}^2 = \frac{a}{2(1-\hat{\varphi})}, \tag{5}$$

$$\hat{\varphi} = \left(\frac{a+2b}{2(a+b)}\right), \tag{6}$$

$$a = \frac{1}{2}\left\{\frac{1}{Y}\sum_{y=1}^{Y}[x_{y1} - x_{y2}]\left[x'_{y1} - x'_{y2}\right] + \frac{1}{Y}\sum_{y=1}^{Y}\left[x_{y2} - x_{y3}\right]\left[x'_{y2} - x'_{y3}\right]\right\}, \tag{7}$$

$$b = \frac{1}{2}\left\{\frac{1}{Y}\sum_{y=1}^{Y}[x_{y1} - x_{y2}][x'_{y2} - x'_{y3}] + \frac{1}{Y}\sum_{y=1}^{Y}[x_{y2} - x_{y3}][x'_{y1} - x'_{y2}]\right\}. \tag{8}$$

In order to reduce the estimation error, the estimated $\hat{\varphi}$ has to be constrained. If both of x_{ym} and x'_{ym} are pressure variables, $\hat{\varphi}$ is constrained to lie within the interval [0, 0.1] (ZF2004). Otherwise (i.e. at least one of x_{ym} and x'_{ym} is a rainfall variable), $\hat{\varphi}$ is empirically constrained to lie within the interval [−0.1, 0.1] (Zheng and Frederiksen 2006).

Since the covariance between two seasonal means can be estimated as

$$V\left(x_{yo}, x'_{yo}\right) \approx \frac{1}{Y-1}\sum_{y=1}^{Y}\left(x_{yo} - x_{oo}\right)\left(x'_{yo} - x'_{oo}\right), \tag{9}$$

the covariance between two seasonal means can be decomposed, using Eq. (4), as

$$V\left(x_{yo}, x'_{yo}\right) = \left[V\left(x_{yo}, x'_{yo}\right) - V\left(\varepsilon_{yo}, \varepsilon'_{yo}\right)\right] + V\left(\varepsilon_{yo}, \varepsilon'_{yo}\right), \tag{10}$$

where the first term on the right-hand side can be rewritten as

$$V\left(x_{yo}, x'_{yo}\right) - V\left(\varepsilon_{yo}, \varepsilon'_{yo}\right) = V\left(\mu_y, \mu'_y\right) + V\left(\mu_y, \varepsilon'_{yo}\right) + V\left(\mu'_y, \varepsilon_{yo}\right), \tag{11}$$

and will be referred to as the "residual" covariance after removing the variability of the intraseasonal component. It is worth emphasizing that this covariance, in general, consists of not only the covariance between μ_y and μ'_y (that is, the slow components of the climate variables), but also their interaction terms with ε_{yo} and ε'_{yo}. In the case where the intraseasonal and slow components are independent, the residual covariance reduces to the covariance of the slow component. When this is not the case, $V(x_{yo}, x'_{yo}) - V(\varepsilon_{yo}, \varepsilon'_{yo})$ may still be better related to the covariance between the two slow components than is $V(x_{yo}, x'_{yo})$.

The covariance matrices for the components of the seasonal mean are adjusted to ensure that they are positive semi-definite using the method described by Grainger et al. (2008).

2.3 Identifying predictable signals

Once the intraseasonal and residual covariance matrices of the seasonal rainfall have been estimated by applying the methodology documented in Sect. 2.2, an empirical orthogonal function (EOF) analysis is conducted to identify the leading modes of each covariance matrix. For convenience, we shall refer to the EOFs of the covariance matrices defined by Eqs. (9), (4) and (11) as the total, intraseasonal or fast and predictable or slow modes of interannual variability in the seasonal mean rainfall. The corresponding principal component (PC) time series of each predictable mode is obtained by projecting the field of 3-month mean (seasonal) precipitation anomalies onto the corresponding EOF mode for each season and year in the time series. The interested reader is referred to ZF2004 for more details.

3 Results

In this section, the leading EOF modes for the predictable component of seasonal precipitation in eastern China for the five consecutive 3-month periods from October–November-December (OND) to February–March–April (FMA). The seasonal variation of these modes will be examined, and the associated possible SST predictors for the most predictable modes will be identified. The atmospheric circulations associated with the potentially predictable modes will be discussed in order to aid the physical interpretation of the predictable rainfall signal. Moreover, interdecadal variations in the relationship between the predictable eastern China rainfall and the SSTs (also the atmospheric circulations) are examined. In addition, leading modes for the intraseasonal component of eastern China rainfall and their associated circulation patterns are shown.

3.1 Interannual variability associated with predictable modes

Before looking into the seasonal variation of the leading predictable rainfall modes, we show in the left column of Fig. 2 the total variance of the rainfall from OND to FMA. Although compared to summer rainfall there is much less rainfall in cold seasons (Li and Ma 2012), the rainfall amplitude displays large interannual variability and its standard deviation can reach 30–50 mm in southeastern China during OND–FMA (Fig. 2a–e), about half of eastern China winter total rainfall. And as can be seen here, from OND to FMA, the total variance of rainfall in the northern part of eastern China is much lower compared to the southern part of eastern China and consists a large south-north spatial gradient, especially in JFM and FMA. The study by Wu et al. (2009) suggested that about 44 % of the variance at these seasons of the year may be explained by two major "seasonal reliant" modes: a post-ENSO mode of which the mono-pole spatial structure is similar to the pattern of the total variance in Fig. 2; and a mode associated with the developing phase of ENSO of which the north–south migration is consistent with the leading predictable mode found in this study as described below.

When looking into the leading predictable rainfall modes from OND to FMA (middle column of Fig. 2), the loadings are localized in a more limited region than that in the total variance maps (left column of Fig. 2), indicating a limited potential predictability in eastern China. This is consistent with Table 1, from which we can see that in most seasons, the intraseasonal component has by far the largest variance compared with the slow component. That is to say, the intraseasonal component is largely responsible for the interannual variance of rainfall in this region, so it is important to do variance decomposition when focusing on the issue of the seasonal predictability. The evolution of the seasonal predictable rainfall modes can also be seen in the middle column of Fig. 2. And at the phase shown here, it is positive loadings that correspond to wet conditions in eastern China. The leading predictable rainfall modes from OND to FMA has a clear north to south seasonal migration (middle column of Fig. 2), and account for more than 60 % of the variance in the slow component (Table 1). In particular, during OND-NDJ, when El Nino develops, the center of maximum amplitude is located in central eastern China close to the region of the Yangtze-Huaihe (YH) river valley. The north to south migration of maximum variation center is consistent with the temporal evolution of the seasonal-reliant EOF mode associated with the developing phase of ENSO at this time of the year as found in Wu et al. (2009). Associated with the north–south maximum rainfall migration, the anomalous wind over south China and the South China Sea changes from south-easterlies in the autumn to early winter to south-westerlies later in the winter. During the boreal winter DJF, as ENSO matures, there are two local maxima in predictable rainfall—one in the YH river valley and another in southeastern China, and then later only one in southeastern China from JFM to FMA. To identify the reason for the two local maxima in predictable DJF rainfall in during entire 1951–2004, the leading DJF predictable mode is estimated for the periods 1951–1977 and 1978–2004 respectively (not shown here). It appears that the one in the YH river valley is only in the mode for 1951–1977, while the one in southeastern China is only in the mode for 1978–2004. Therefore, the two local maxima are related to decadal variability that will be discussed in Sect. 3.4.

In order to have a better understanding of the causes of the predictability, we calculated the correlations between leading predictable rainfall PCs and 1-season lead SSTs (e.g. the SST of JAS and the rainfall PC of OND). As shown in the right column of Fig. 2, the lag-lead correlations between slow rainfall PCs and SSTs show similar characteristics from OND to FMA. A noticeable feature

Fig. 3 Slow covariance maps of 500 hPa height field associated with► predictable rainfall modes for five consecutive 3-month periods from late-fall (OND) to early spring (FMA). The covariance is calculated for the periods of 1951–2004 (*left*), 1951–1977 (*center*), and 1978–2004 (*right*), respectively

Table 1 Variability of total, intraseasonal and slow component of the seasonal rainfall pattern (left three columns; unit: mm^2), the potential predictability of seasonal precipitation (the fourth column), and the variance of respective components explained by the seasonal precipitation's slow- and intrseasonal- PCs (right four columns).

Season	Total var.	Intra var.	Slow var.	S/T	% Explained var.			
					S-PC1 (%)	S-PC2 (%)	I-PC1 (%)	I-PC2 (%)
OND	54,790	46,383	8,407	0.15	68	9	31	12
NDJ	34,634	28,779	5,855	0.17	77	10	42	12
DJF	32,423	28,789	3,635	0.11	63	17	49	18
JFM	55,906	40,205	15,701	0.28	83	6	46	11
FMA	83,205	69,525	13,680	0.16	69	9	34	16

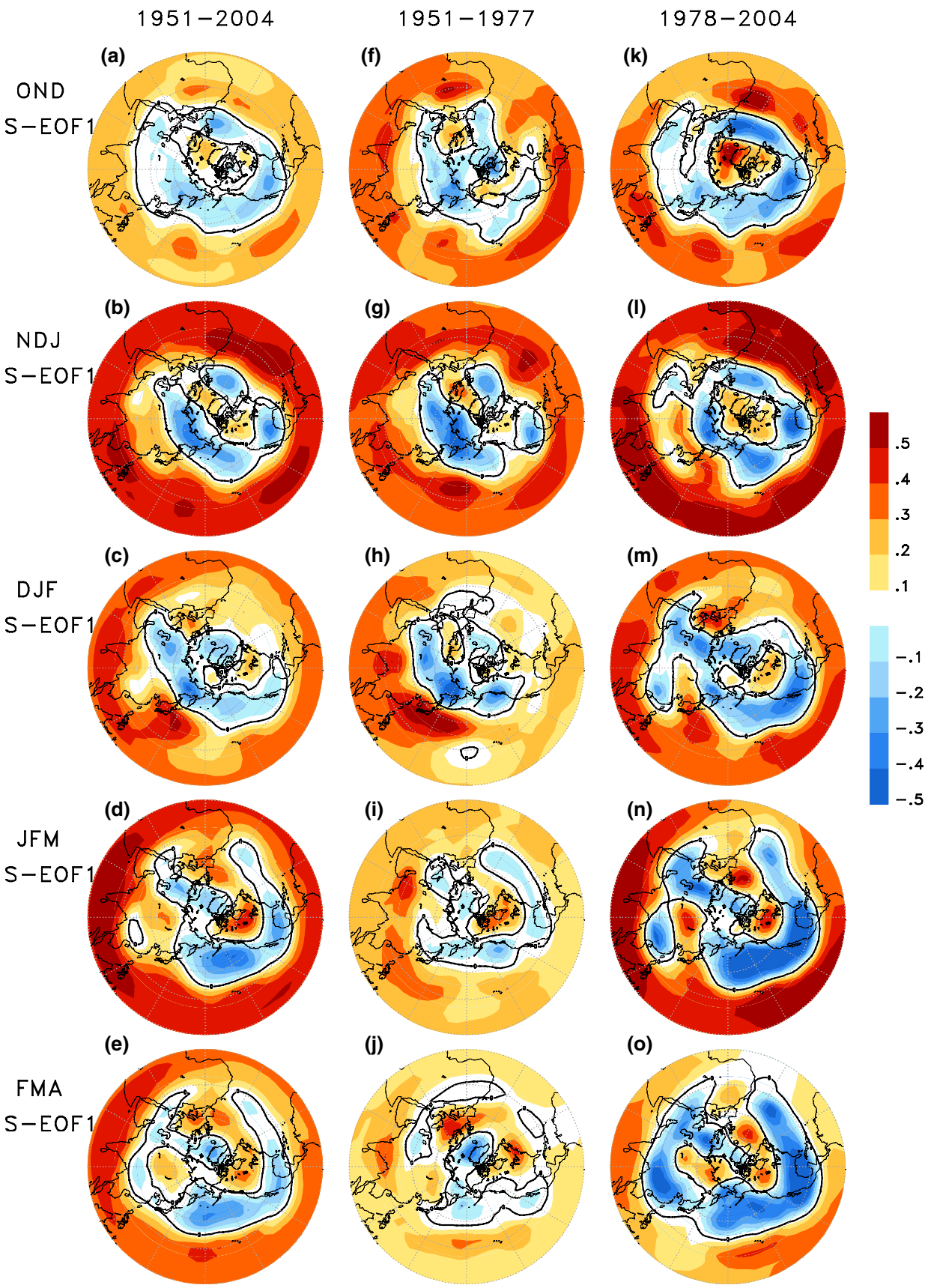
1951–2004
1951–1977
1978–2004
(a)
(f)
(k)
OND
S–EOF1
(b)
(g)
(l)
NDJ
S–EOF1
(c)
(h)
(m)
DJF
S–EOF1
(d)
(i)
(n)
JFM
S–EOF1
(e)
(j)
(o)
FMA
S–EOF1
.5
.4
.3
.2
.1
–.1
–.2
–.3
–.4
–.5

that appears in the SST correlation patterns is the maximum values in the eastern tropical Pacific Ocean, which indicates that the predictable rainfall patterns are associated with the El Nino/Southern Oscillation (ENSO). Negative correlations in the tropical western Pacific during the late-fall become much weaker in winter. Previous studies provided by Zhang et al. (1999), Wu et al. (2003) and Zhou et al. (2010) showed that seasonal rainfall anomalies in eastern China have correlations with concurrent and lead-lag Nino-3 SST anomalies during the fall of an ENSO developing year through the following spring. Our analysis indicates that these anomaly patterns are also the dominant seasonally predictable patterns, consistent with the results of studies by Wu et al. (2009) and Zhou et al. (2009a). Furthermore, the correlations between our predictable precipitation patterns and ENSO are much stronger during autumn seasons (OND–NDJ) than that in winter seasons (DJF–FMA). The possible reasons for this seasonal variation of correlations will be discussed in the following sections.

3.2 Circulation patterns associated with the predictable modes

In order to aid the physical interpretation of our slow rainfall modes and understand the atmospheric teleconnections between precipitation anomalies and ENSO, we will examine the atmospheric circulations associated with the predictable rainfall modes. We do this by estimating the covariance between the PC time-series of the slow rainfall EOFs and the slow component of the circulation field, using Eq. (11). These slow covariance patterns are associated with very slowly varying (interannual to supra-annual) external forcing and internal dynamics (Frederiksen and Zheng, 2004), which could help in identifying possible circulation predictors for forecasting rainfall.

The left column of Fig. 3 shows the slow covariance of 500-hPa geopotential height associated with the predictable rainfall modes from OND to FMA at the phase shown in Fig. 2. In each season, the covariance patterns display a largely zonally symmetric structure. There are positive values all over the broad tropical region, negative height anomalies occur in mid- to high-latitudes, and weak positive height anomalies are seen over the region of the North Pole. The positive center in the tropics is mainly situated from the east side of the Philippines to the east coastline of Africa with the latitude between 10 and 20°N. This is the area most affected by the descending branch of the Hadley cell (Quan et al. 2004a, Fig. 3) and the western Pacific subtropical high (WPSH), indicating that these may be important factors affecting east China rainfall. In particular, as the Hadley cell circulation intensifies and the WPSH becomes stronger and extends anomalously more westward, more moisture is brought in from the south into eastern China and cause wetter than normal conditions as seen in Fig. 4 (left column) which shows covariance between the temporal variation of the leading predictable mode and the 850 hPa wind. A similar depiction of the circulation pattern of low level wind and vertical velocity over the western Pacific and east Asia monsoon region during with the developing phase of ENSO is also found in Wu et al. (2009, Fig. 7). The relationship between the predictable rainfall modes and the WPSH was further examined using composite maps of 500 hPa geopotential height associated with predictable rainfall modes during the cool seasons (Figures not shown here), and the results are consistent. It is also consistent with the findings of Zhang et al. (1999).

Other noticeable features in the atmospheric circulation, associated with the most predictable rainfall mode, are the teleconnection patterns in the extra tropics. During the seasons of OND, NDJ and DJF (Fig. 3a–c), this pattern is similar to the Slow-REOF3 seen in Fig. 4 of Frederiksen and Zheng (2004) identified as the Western Pacific Oscillation (WPO), which is significantly related to tropical SST variability associated with ENSO. The relatively weaker magnitude of the covariance in the earlier autumn (OND) is attributed to the seasonality of atmospheric response to ENSO forcing (e.g. Quan et al. 2004b). From JFM to FMA (Fig. 3d, e), the covariance pattern associated with slow-EOF1 shows large amplitude over the North Pacific/North American region with a structure similar to the Pacific North American (PNA) teleconnection pattern of Frederiksen and Zheng (2004, Fig. 4, Slow-REOF2), which is also related to ENSO. So teleconnections found between the predictable rainfall modes and circulation varies with the change in seasons. Generally, the WPO is associated with the slow component of rainfall in eastern China in autumn seasons (OND to DJF), and the PNA from JFM to FMA. This indicates that beside the WPSH, the predictable rainfall variability is also driven by the larger scale hemispheric circulation patterns.

3.3 Interannual variability associated with intraseasonal variability

Our main aim in this study has been to identify and understand the seasonal predictable signals of precipitation in eastern China. However, from Table 1 it is clear that interannual variability of east China rainfall is largely related to the intraseasonal component. It is therefore of interest to consider how intraseasonal variability influences, or can generate, coherent patterns of interannual variability. The two dominant intraseasonal modes from OND to FMA are shown in Fig. 5. They explain more than 50 % of the variance in the intraseasonal component in each season. The anomalous circulation associated with both fast modes has a more wavy structure, in contrast to the leading slow

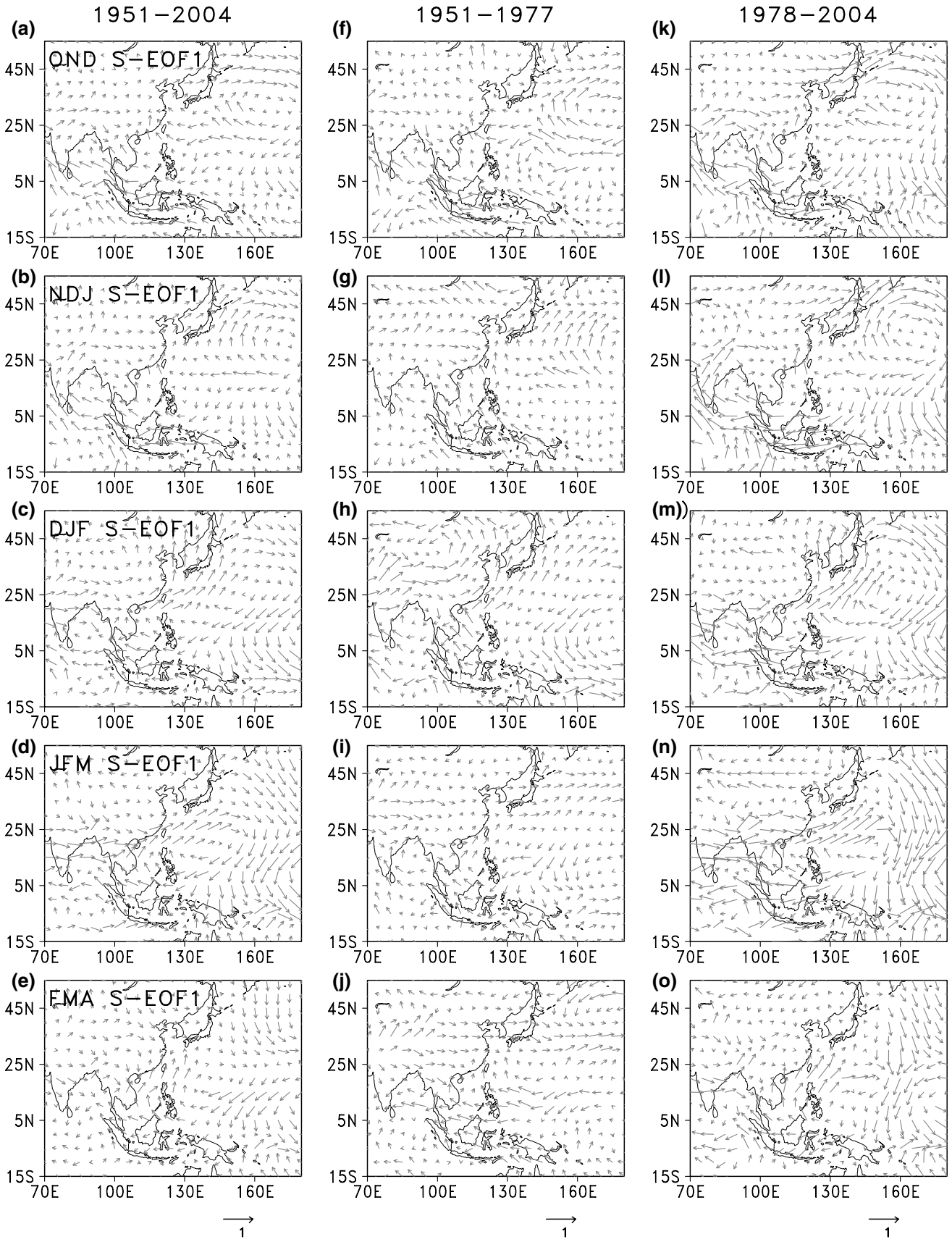

Fig. 4 Slow covariance maps of 850 hPa wind field associated with the leading slow mode, of the rainfall in east China from late-fall (OND) to early spring (FMA) during the years of 1951–2004 (*left*), 1951–1977 (*center*), and 1978–2004 (*right*), respectively

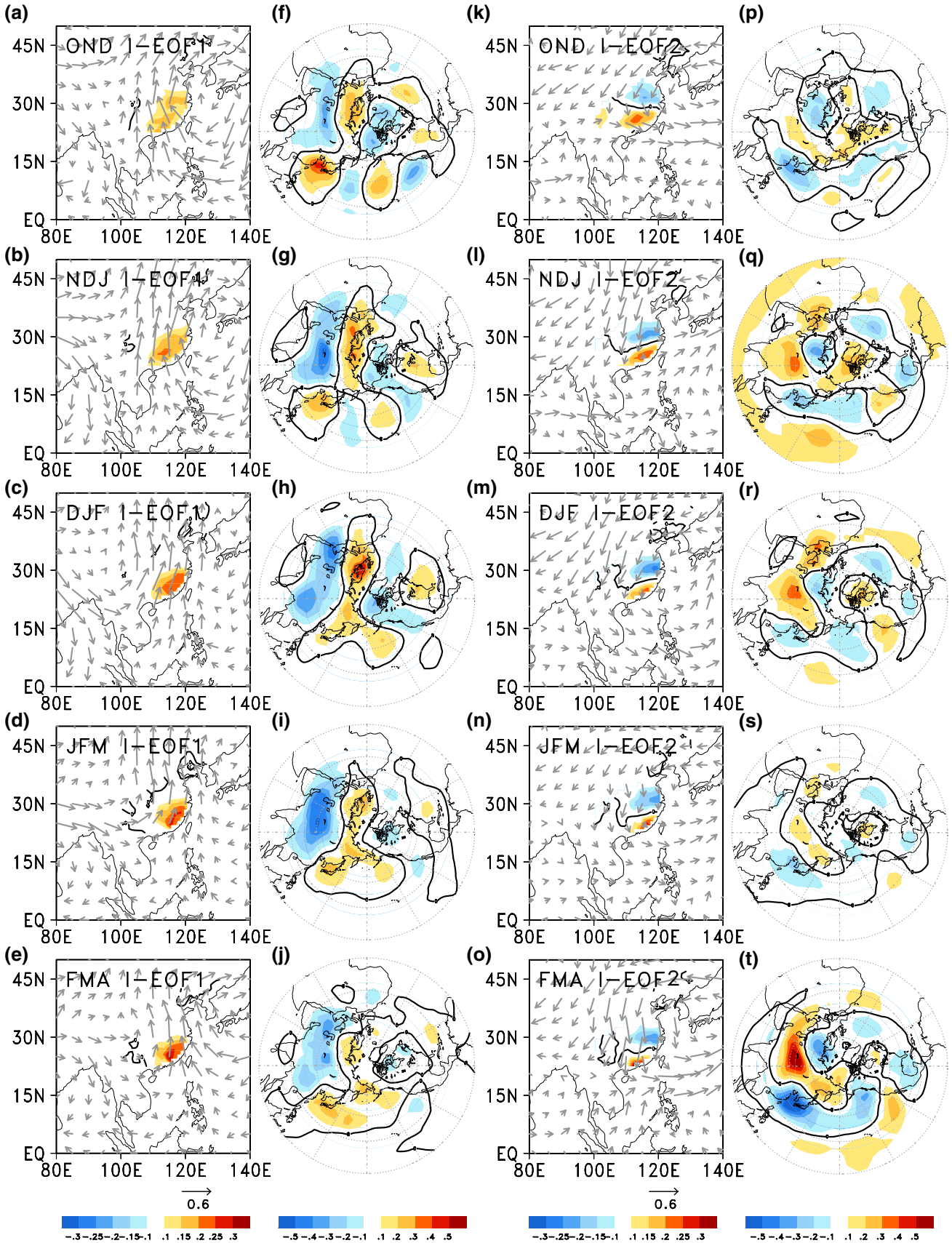
(a)
OND I−EOF1
(b)
NDJ I−EOF1
(c)
DJF I−EOF1
(d)
JFM I−EOF1
(e)
FMA I−EOF1
(f)
(g)
(h)
(i)
(j)
(k)
OND I−EOF2
(l)
NDJ I−EOF2
(m)
DJF I−EOF2
(n)
JFM I−EOF2
(o)
FMA I−EOF2
(p)
(q)
(r)
(s)
(t)
45N
30N
15N
EQ
80E
100E
120E
140E
0.6
−.3 −.25 −.2 −.15 −.1 .1 .15 .2 .25 .3
−.5 −.4 −.3 −.2 −.1 .1 .2 .3 .4 .5

◂**Fig. 5** Spatial patterns of the 1st and 2nd fast (intraseasonal) modes and the covariance between the associated time series for the intraseasonal rainfall mode and the intraseasonal component of 500 hPa wind field (*rectangular panels*) and intraseasonal covariance maps of 500 hPa height field associated with intraseasonal rainfall modes for the seasons from late fall (OND) to early spring (FMA). The covariance is calculated for the periods of 1951–2004

mode which is more zonally symmetric. Also, unlike the associated slow circulation, the circulation pattern does not change much between the seasons.

The leading fast EOFs in all seasons (Fig. 5a–e) show similar structures with positive loading everywhere, and a maximum centered in southeastern China. These are more spatially broad than the predictable EOFs and more like the total variance patterns shown in the first column of Fig. 2. The covariance between the intraseasonal component of the 500-hPa geopotential height and the 1st intraseasonal rainfall modes is also examined in Fig. 5f–j. In all five seasons, at the particular phase shown, the covariance patterns associated with the most dominant mode of variability has large positive loadings in Japan and northern Europe in the high latitudes north of about 60°N, and negative loadings in the broad Eurasian continent along with a weakened Siberian High. There is also a PNA-like pattern over North America. This spatial structure is quite similar to the Intraseasonal-REOF2 pattern shown in Frederiksen and Zheng (2004, Fig. 3), associated with the intraseasonal Madden-Julian Oscillation. The circulation features suggest that positive anomalies over south eastern China are associated with more moisture coming from the Philippine Sea.

The second intraseasonal EOFs of the rainfall in eastern China have a similar south-north dipole structure in all the seasons examined in Fig. 5k–o. At the phase shown, the southeast China has wetter-than-normal conditions in the south and drier conditions in the north. The 500 hPa height pattern associated with the second intraseasonal EOFs in these seasons (Fig. 5p–t) have some WPO-like patterns associated with trough (block) in the western North Pacific and intensified (weakened) Siberian High (see I-REOF3 in Fig. 3 of Frederiksen and Zheng 2004). The 500 hPa height pattern shown in Fig. 5 is accompanied by anomalous northerlies over the east China and anomalous westerlies or southwesterlies over the southern coastline of China and the South China Sea, resulting in drier-than-normal conditions over the north of the southeast region of China and wetter conditions in the south.

Our further analysis indicates that the two fast rainfall EOF modes are not sensitive to the intraseasonal variations in SST conditions (figure not show). Instead the two fast modes are manifestation of the intraseasonal variabilities of the Siberian High over the Eurasian continent and the western Pacific subtropical high associated with the WPO-like intraseasonal variability over the North Pacific. Figure 6 examines the covariance between the two fast rainfall modes and the fast components of the temporal variabilities of OLR and 500 hPa wind field. Neither of the two fast rainfall modes have apparent connection to ENSO. Again, the first fast mode is more related to the anomalous condition of Siberian High, while the second fast mode appears to be associated with stronger WPO-like anomalies over the western Pacific.

3.4 Interdecadal change in the precipitation: ENSO correlation

To investigate if there are interdecadal shifts in the relationship between the predictable precipitation in the eastern China and the SSTs in winter and autumn (OND–FMA) around late 1970s, we compare the lead-lag SST correlation associated with the predictable rainfall PCs between 1951 and 1977 (negative PDO epoch, according to the evolution of PDO index by Mantua et al. 1997; shown in the left column of Fig. 7) and 1978–2004 (positive PDO epoch; shown in the right column of Fig. 7).

Figure 7 shows that there is an apparent seasonality in the behavior of the correlation between the east China's slow varying precipitation and ENSO at the interdecadal time-scale. Strong precipitation-ENSO correlations are seen in both the sub-periods for the seasons of OND to NDJ (Fig. 7, top two rows). In contrast, interdecadal changes in the precipitation-ENSO correlation are apparent for DJF to FMA in that the correlation is much stronger in the later period 1978–2004 (Fig. 7, bottom three rows).

What is the cause of this seasonality in the interdecadal change of the relationship between ENSO and the seasonal precipitation in east China? It has been widely noticed that a distinct interdecadal change had occurred in the connection between the summer precipitation in east China and ENSO (e.g. Chang et al. 2000; Wu and Wang 2002; Xie et al. 2010; Yun et al. 2010; Wu et al. 2011). The change has been attributed primarily to two mechanisms: (1) change in the life-cycle of an ENSO event (Chang et al. 2000); and (2) change in the prevailing ocean surface condition and associated atmospheric circulation pattern (Wu and Wang 2002). The study by Wang et al. (2008a, b) suggested that the relationship between ENSO and the western North Pacific, East Asian, and Indochinese monsoons had become enhanced attributing to increased magnitude and periodicity and strengthened monsoon-ocean interaction. Following the considerations of these previous studies, we checked the interdecadal changes of the subtropical high and the seasonality of the intensity of ENSO signals between the two multi-decadal periods of 1951–1977 and 1978–2004. We found that the subtropical high was intensified and extended more westward in the period of 1978–2004 in all periods from OND to FMA (figure not shown)

probably due to SST warming in the tropical Indian and western Pacific oceans by the mechanism as suggested in the study of Zhou et al. (2009c). The fact that the subtropical high has intensified in both the fall and winter but the rainfall-ENSO relation is strengthened only in winter indicates that some other factor is more dominant to make the interdacedal change of the rainfall-ENSO relation particularly large in winter.

Results of our analysis suggest that the seasonality seen in Fig. 7 is well explained by the change of the intensities of the ENSO signals in different seasons. The results are illustrated in the following three figures. Seasonality in the interdecadal changes of the intensity of ENSO signal in SST is illustrated in Fig. 8. This shows the differences between the composites of SST anomalies in El Niño years and those in La Niña years. The SST signal is apparently larger in NDJ than in JFM during 1951–1977 (Fig. 8, top row). The differences in these two periods become much less apparent during 1978–2004 (Fig. 8, bottom row) because the ENSO SST signal is stronger. For example, the Nino3.4 (5S–5 N, 170–120 W) SST anomalies increased from 2.1 to 2.8 C in NDJ and from 1.7 to 2.3 C in JFM. More importantly, the atmospheric response to the change in ENSO SST is nonlinear as we may see in the corresponding change of tropical precipitation shown in Fig. 9. Consistent with the weaker SST signal in JFM in the early period, the ENSO signal in precipitation was also much weaker in JFM than in NDJ during 1951–1977. In contrast, the ENSO precipitation signals are of similar intensity during 1978–2004. In the region of Nino3.4, the precipitation signal increased about 46 % from 2.6 mm/day (1951–1977) to 3.8 mm/day (1978–2004) in NDJ. A much larger increase of 140 % from 1.5 to 3.6 mm/day had occurred in JFM.

A similar pattern of the interdecadal change is also observed in the precipitation in east China (Fig. 10). These patterns are obtained from the CMA's archive of station observations, a data source that is completely independent from the NCEP/NCAR's precipitation reanalysis used in Fig. 9. The consistency between the seasonalities of precipitation changes shown in Figs. 9 and 10 provides a strong evidence supporting the argument that the seasonality in the interdecadal change of ENSO signal is real; and the seasonality in the interdecadal change of the correlation between ENSO and the seasonal precipitation in east China is a manifestation of the seasonality in the interdecadal change of the ENSO signal.

Atmospheric circulation associated with the interdecadal change in the rainfall-ENSO relation is examined in the middle column and the right column of Fig. 3 which presents the slow covariance of the 500-hPa geopotential height corresponding to the predictable rainfall modes from OND to FMA before and after the late 1970s, respectively.

Fig. 6 Covariance between the time series of first (*left column*) and second (*right column*) fast rainfall EOF modes and the fast component of the time series of OLR (*colored shading*), and 500 hPa wind field (*vectors*)

During DJF–FMA, the slow covariance pattern shows remarkable differences between the two periods over the broad tropical region: in 1978–2004 (Fig. 3m–o), higher covariance has been observed compared to 1951–1977 (Fig. 3h–j). In contrast, during OND–NDJ, the 500-hPa height covariance had increased only moderately. The seasonality in the change of rainfall-height covariance is consistent with the seasonality in the change of ENSO signal seen in Figs. 7, 8, 9, 10. The generally zonally symmetric pattern in the increased height covariance in the tropical area from DJF to FMA implies an intensified Hadley cell circulation. This is consistent with the studies by Quan et al. (2004a) that the winter (DJF) Hadley cell has increased in intensity since 1950s partly due to the variation of SST in the tropical oceans and the global warming. Corresponding changes in the slow covariance of the 850 hPa wind is further examined in the middle and the right column of Fig. 4. As expected, changes in the covariance of wind field is much more significant in the winter than in the fall seasons, also consistent with the seasonality in the change of ENSO signal. It is worth to note that the intensified anticyclonic pattern over the subtropical western north Pacific seen in the winter of 1978–2004 is a feature of enhanced variability but not a change of the mean state. And our analysis shown in this section suggests that the winter strengthening of rainfall-ENSO relation is better explained by the enhanced SST and atmospheric variabilities associated with ENSO rather than the changes in mean states of ENSO SST and the western North Pacific subtropical high, although the later has been regarded as a major factor in explaining the interdecadal change/variations of rainfall and temperature pattern in east China (e.g. Zhou et al. 2008; Li et al. 2010a, b; Zhou et al. 2013; Qian and Zhou 2014). We also noticed that some large changes in the covariance of wind field also occurred over the eastern tropical Indian ocean in the seasons of late autumn to winter. Whether the change over the tropical Indian ocean during this time of the year can be explained by the mechanism for summer as suggested by Xie et al. (2010) is an interesting open question.

4 Summary and discussion

In this study, we have applied the variance decomposition method of Zheng and Frederiksen (2004, ZF2004 in short) to identify more predictable signals of seasonal mean precipitation in eastern China during cool seasons (from OND

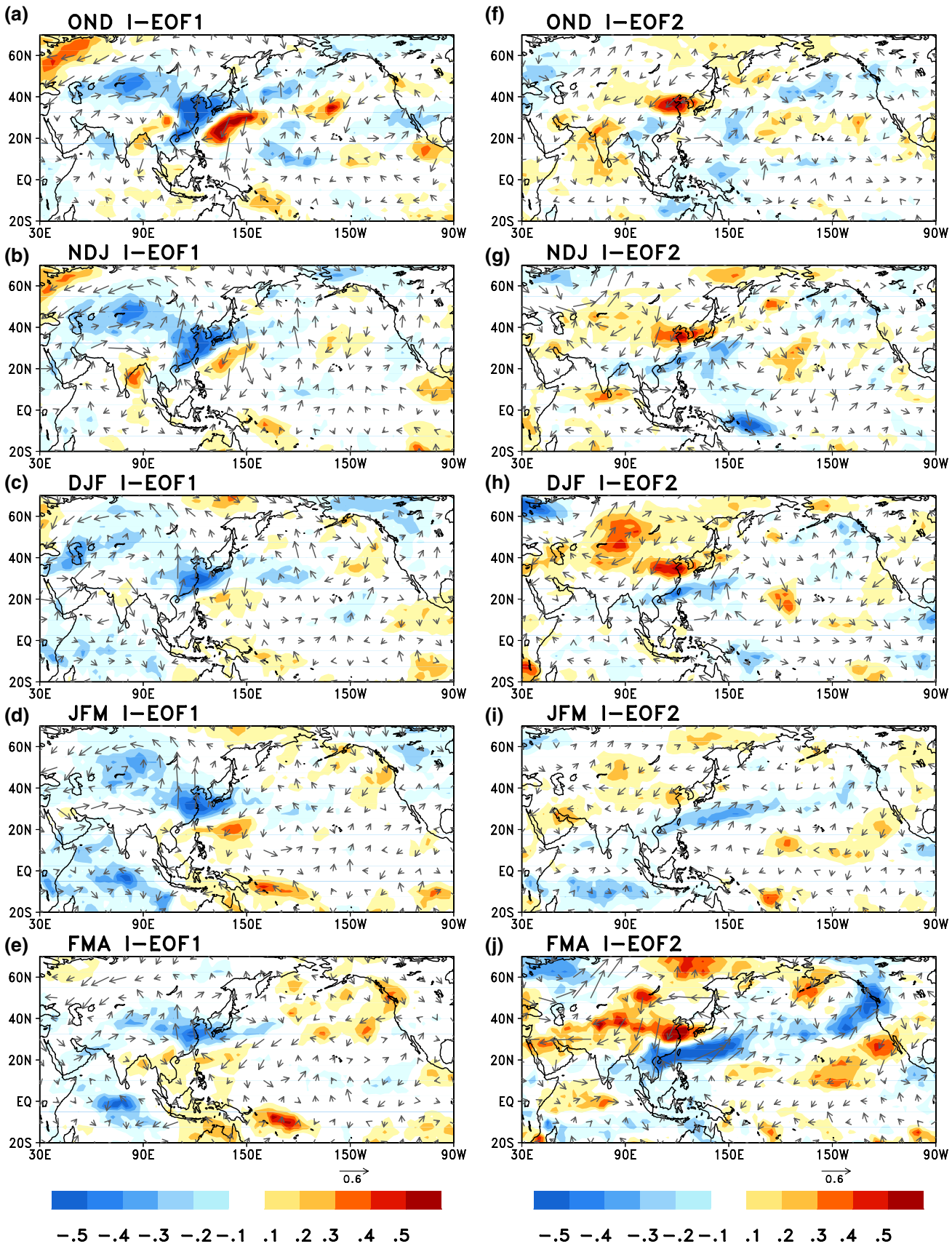
(a) OND I−EOF1
(b) NDJ I−EOF1
(c) DJF I−EOF1
(d) JFM I−EOF1
(e) FMA I−EOF1
(f) OND I−EOF2
(g) NDJ I−EOF2
(h) DJF I−EOF2
(i) JFM I−EOF2
(j) FMA I−EOF2
60N
40N
20N
EQ
20S
30E
90E
150E
150W
90W
0.6
−.5 −.4 −.3 −.2 −.1 .1 .2 .3 .4 .5

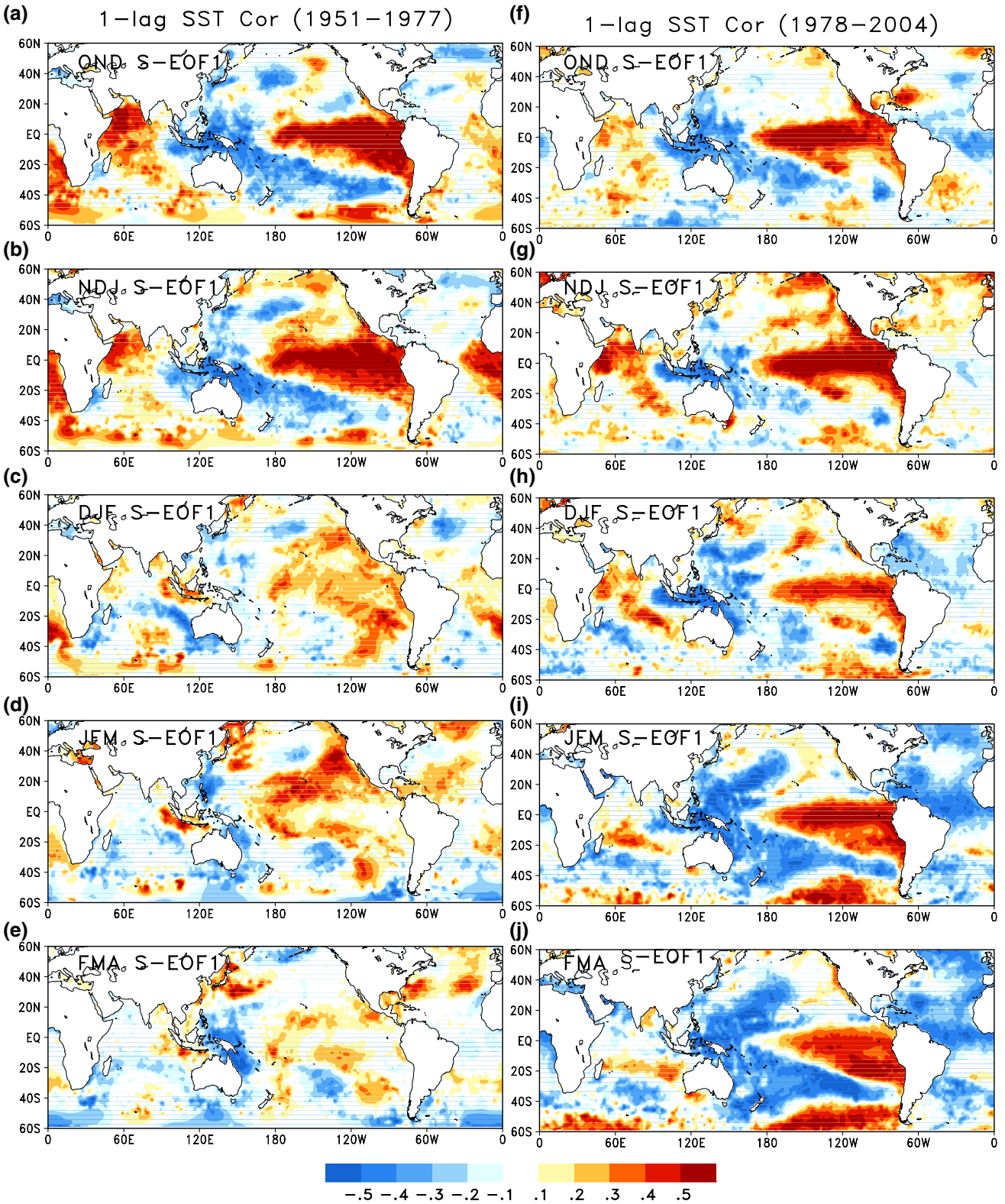

Fig. 7 Spatial patterns of 1-season lag correlation between PC time series of the leading slow mode and SST for the five consecutive 3-month periods from late-fall (OND) to early spring (FMA) during the years of 1951–1977 (*left*) and 1978–2004 (*right*)

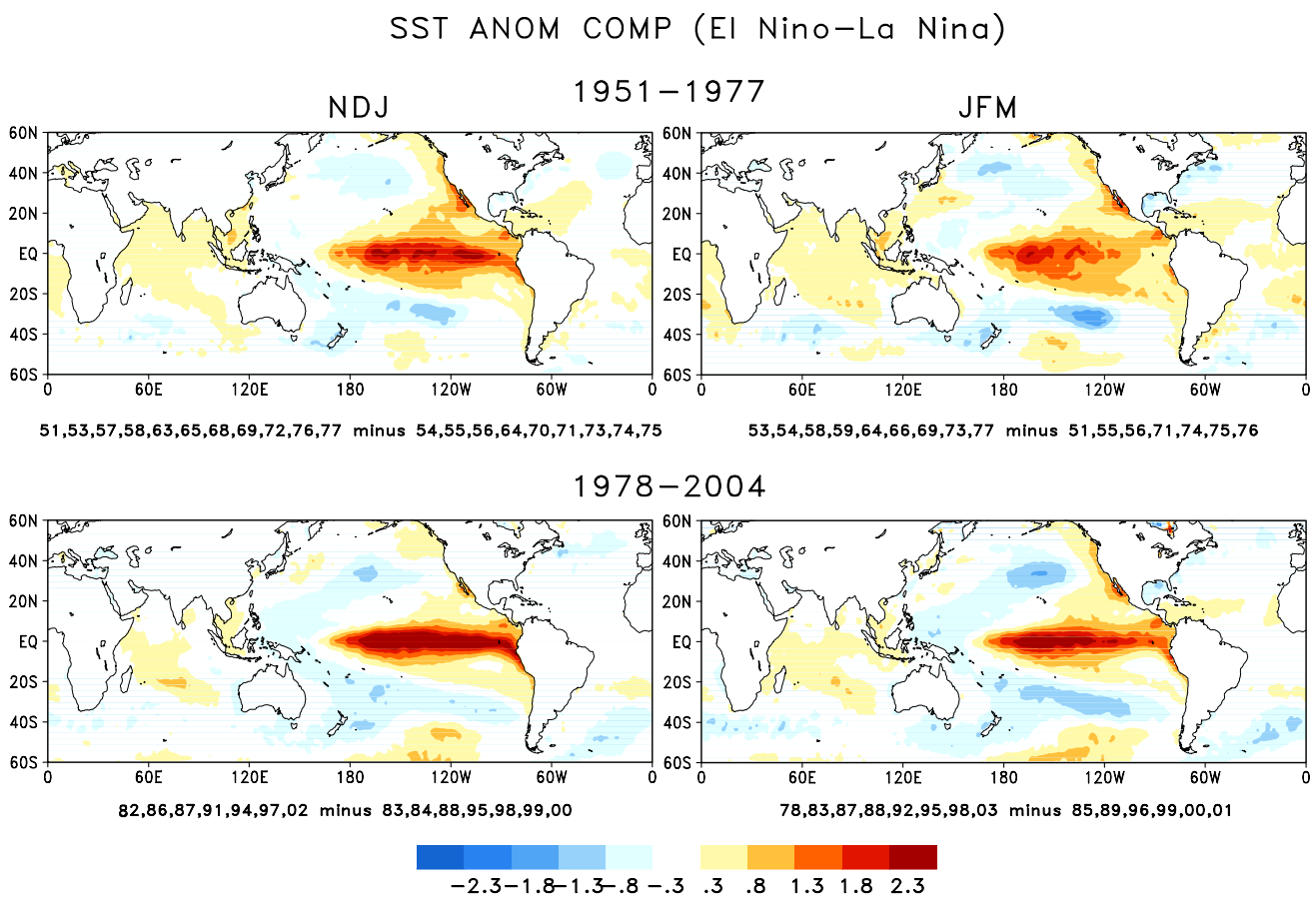

Fig. 8 Composites of SST anomalies for the 3-month period of NDJ (*left*) and JFM (*right*) during the years of 1951–1977 (*top*) and 1978–2004 (*bottom*). El Niño (*warm*) and La Niña (*cold*) events are defined when a threshold of ±0.5 °C for oceanic Niño index (ONI; from NOAA Climate Prediction Center) is met for a minimum of five consecutive over-lapping seasons

to FMA). Using the ZF2004 method, the covariance matrix of eastern China seasonal mean rainfall fields has been decomposed into covariance matrices associated with the intraseasonal and slow components of the rainfall, with the latter related to the potentially predictable signal. With this approach, we have gained a more quantitative understanding of the source of predictability and uncertainty in eastern China rainfall variability.

The analysis shows a robust influence of ENSO on the seasonal predictable rainfall signal in eastern China during boreal cool seasons. Predictable rainfall modes associated with ENSO show a seasonal evolution. In OND–NDJ maximum loading is in the region of the Yangtze-Huaihe River Valley; in DJF, there are two local maxima—one in YH and the other in southern China; in JFM–FMA maximum loading is in southeastern China. The spatial structure of the leading slow mode consists of center(s) of maximum anomalies that migrates from the southern flank of the Yangtze-River Valley in fall to the coastline of south China in winter. In contrast, the spatial structures of the leading fast modes are relatively stationary.

Teleconnections have been examined between the predictable ENSO-related rainfall modes and the circulation. It is found that the covariance of anomalous atmospheric circulation associated with the leading slow mode appears to be rather zonally symmetric especially in the tropics. The implied variability in the Hadley Cell circulation and the western Pacific subtropical high play an important role on eastern China precipitation. In particular, as the Hadley cell circulation intensified and the western Pacific subtropical high becomes stronger and extends anomalously more westward, more moisture is brought in from the south into eastern China and cause wetter than normal conditions. Teleconnection patterns of the atmospheric circulation are also highly related to the predictable modes of the seasonal rainfall in eastern China, with the western Pacific subtropical high being a key part of larger scale hemispheric circulation patterns.

The intraseasonal (fast) component of the interannual variability in the rainfall in east China consists two major modes, one has a monopole structure that varies uniformly in the southeast China while the other has a north–south

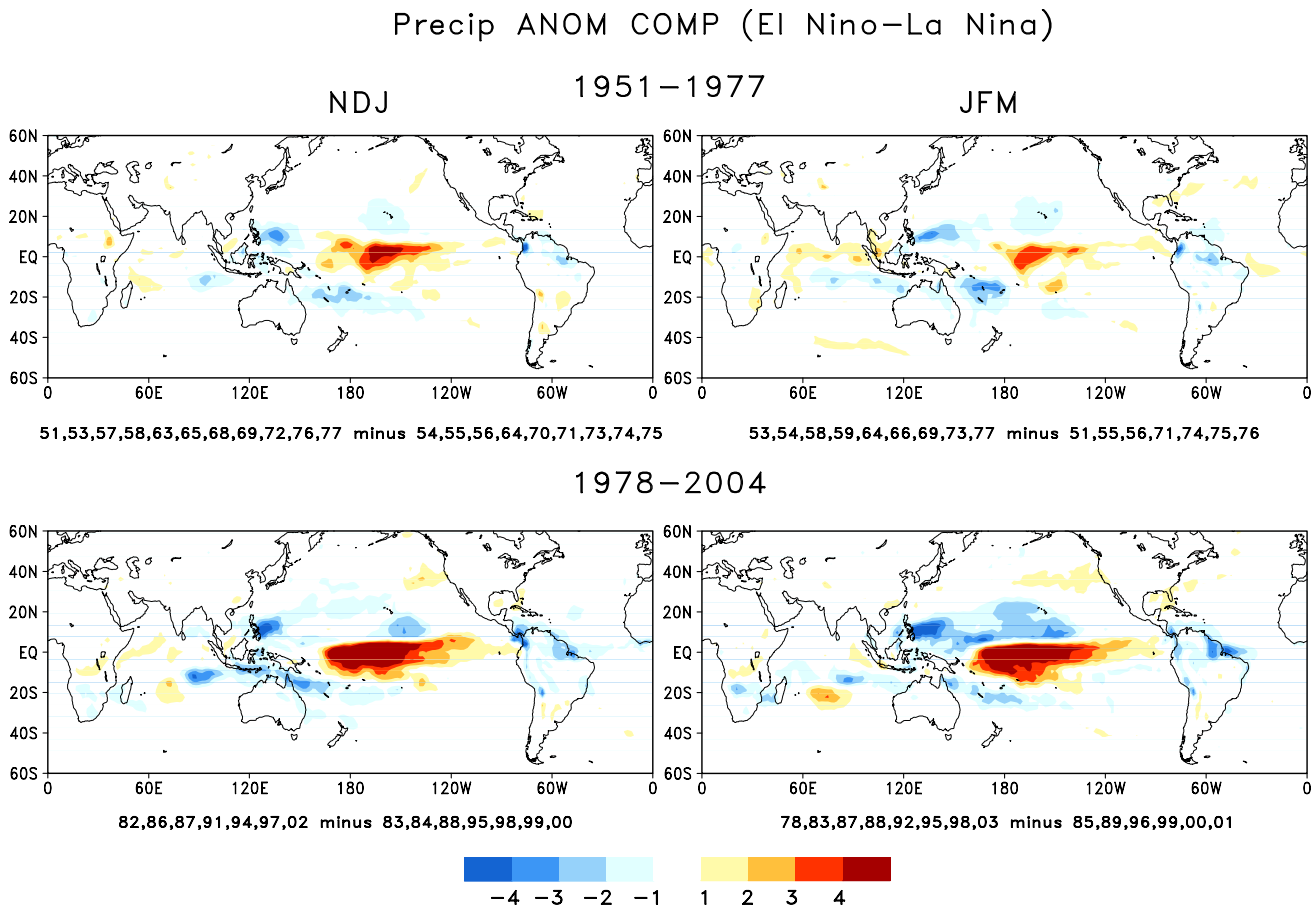

Fig. 9 Composites of tropical precip. anomalies (unit: mm/day) for the 3-month period of NDJ (*left*) and JFM (*right*) during the years of 1951–1977 (*top*) and 1978–2004 (*bottom*)

oriented dipole structure. Atmospheric circulation anomalies associated with the two leading modes of the intraseasonal components of rainfall variability are of wavy structure reflecting the well-known NH circulation features associated with intraseasonal. Further analysis of the convariance between the fast rainfall modes and the fast temporal variabilities of OLR and wind field indicate that the first fast rainfall mode is more a reflection of the anomalous condition of the Siberian High over the Eurasian continent while the second fast rainfall mode is better connected to the intraseasonal variability having WPO_like pattern over the North Pacific Ocean.

Interdecadal change of the rainfall-ENSO relationship were examined by comparing the correlation between 1951–1977 and 1978–2004. A pronounced difference in correlation was found in the eastern tropical Pacific Ocean during winter seasons (DJF to FMA). In particular, significant positive correlations appear during 1978–2004 while the lead-lag relationship is very weak during 1951–1977. In contrast, the apparent positive correlation between ENSO and predictable rainfall modes in eastern China holds in the two shorter periods during autumn seasons (OND to NDJ). Further examination found the significant interdecadal change maybe attributed to an increased intensity of ENSO, and more vigorous atmospheric responses including an intensified variabilities in the tropical Hadley Cell circulation and the western Pacific subtropical high, larger ENSO signal in the winter rainfall in east China and the strengthened covariance between the atmospheric circulation and the rainfall variabilities.

Some previous studies have suggested that the connection between the East Asia winter monsoon and ENSO has weakened (e.g. Wang and He 2012; Chen et al. 2013). The difference may come from the different definitions of the East Asia monsoon used in the previous studies. For example the study by Wang and He (2012) used the regional mean of the 500 hPa over east Asia (25–45°N, 110–145°E) as an index of the East Asia winter monsoon which is better associated with cold surge activity but not so to the variations of precipitation in this region. The difference may also come from the region of SST in

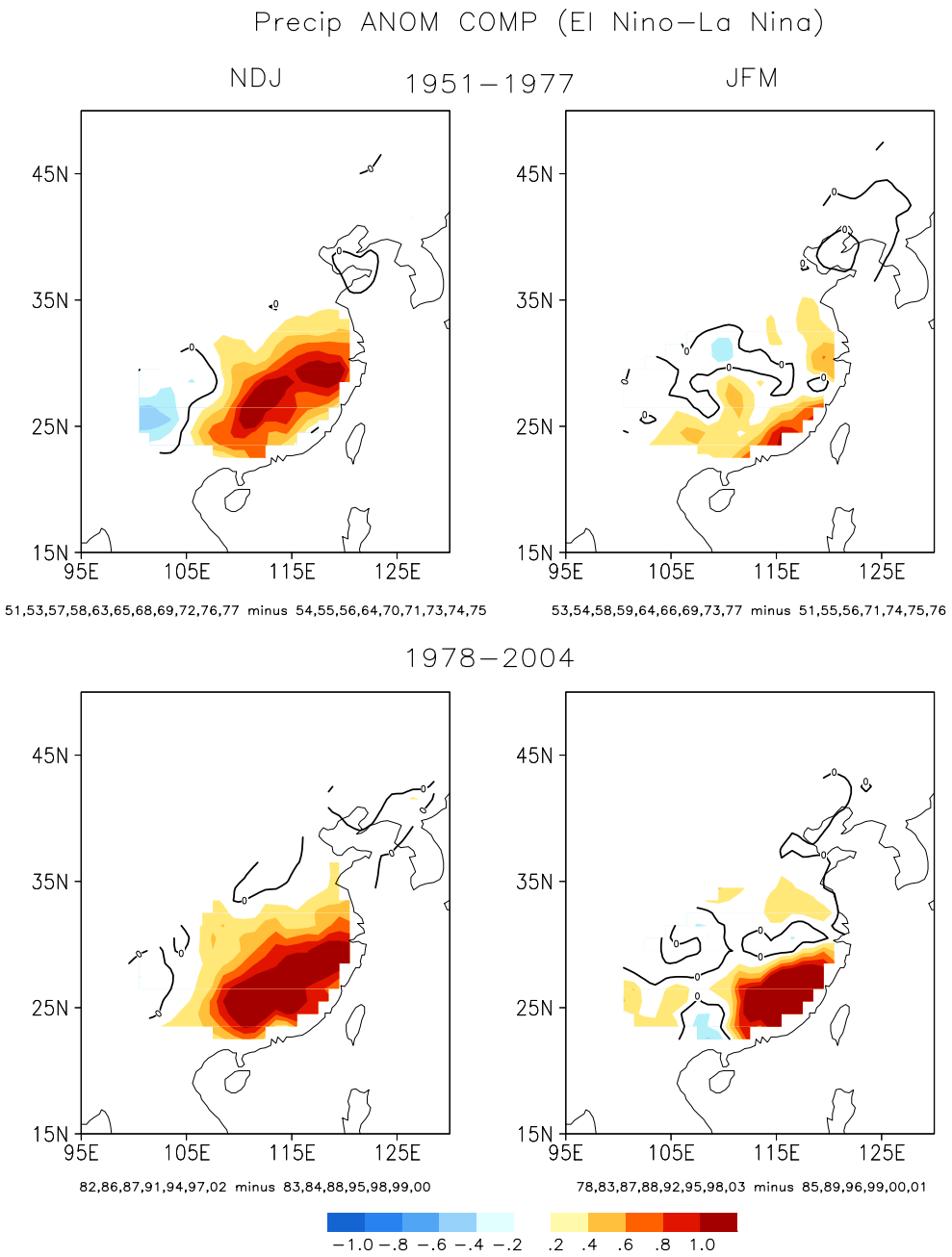

Fig. 10 Composites of east China precip. anomalies (unit: mm/day) for the 3-month period of NDJ (*left*) and JFM (*right*) during the years of 1951–1977 (*top*) and 1978–2004 (*bottom*)

concern. For example, in the study by Chen et al. (2013), the correlation between the winter-spring precipitation in south China and the SST of Nino4 decreased while the correlation with Nino3 and Nino3.4 increased (cf. Fig. 1 in Chen et al. 2013). However, our result is consistent with the previous authors in that the ENSO impact in the winter season is mostly seen in the south China. Because the subtropical high over the North Pacific Ocean is in its southern most location, no significant ENSO impact is detected in the interannual variability of seasonal precipitation in the Yangtze and Huaihe Rivers valley at this time of the year (Ying et al. 2013).

Acknowledgments This work was supported by National Program on Key Basic Research Projects of China (Grant No. 2010CB951604), National Basic Research Program of China (Grant No. 2012CB956203), and Key Technologies Research and Development Program of China (Grant No. 2013BAC05B04). The authors thank the anonymous reviewers of this paper whose informative and

insightful comments/suggestions have bean very helpful and greatly improved the quality of the paper. We also grateful to the editors for their hard work and suggestions on this manuscript.

References

Chang CP (2004) The East Asian monsoon. World Scientific, Singapore

Chang CP, Zhang Y, Li T (2000) Interannual and interdecadal variations of the East Asian summer monsoon and tropical Pacific SSTs. Part II: meridional structure of the monsoon. J Climate 13:4326–4340

Chen JP, Wen ZP, Wu RG, Chen ZS, Zhao P (2013) Interdecadal changes in the relationship between Southern China winter-spring precipitation and ENSO. Clim Dyn. doi:10.1007/s00382-013-1947-x

Ding YH (1994) Monsoons over china. Kluwer Academic Publishers, The Netherlands

Ding YH, Chan JCL (2005) The East Asia summer monsoon: an overview. Meteorol Atmos Phys 89:117–142. doi:10.1007/s00703-005-0125-z

Frederiksen CS, Zheng XG (2004) Variability of seasonal-mean fields arising from intraseasonal variability: part 2, application to NH winter circulations. Clim Dyn 23:193–206

Frederiksen CS, Zheng X (2007) Coherent patterns of interannual variability of the atmospheric circulation: the role of intraseasonal variability. In: Denier J, Frederiksen JS (eds) Frontiers in turbulence and coherent structures, World scientific lecture notes in complex systems, vol 6. World Scientific, Singapore, pp 87–120

Grainger S, Frederiksen CS, Zheng XG (2008) A method for evaluating the modes of variability in general circulation models. ANZIAM J 50:C399–C412

He C, Zhou T, Zou L, Zhang L (2013) Two interannual variability modes of the Northwestern Pacific Subtropical Anticyclone in boreal summer. Sci China Earth Sci 2013(56):1254–1265. doi:10.1007/s11430-012-4443-y

Hsu HH, Zhou T, Matsumoto J (2014) East Asian, Indochina and Western North Pacific summer monsoon-an update. Asia Pacific J Atmos Sci 50(1):45–68

Hu ZZ (1997) Interdecadal variability of summer climate over East Asia and its association with 500 hPa height and global sea surface temperature. J Geophys Res 102(19):403–412

Huang RH, Sun FY (1994) Impacts of the thermal state and the convective activities in the tropical western Pacific warm pool on the summer climate anomalies in East Asia. Scientia Atmospherica Sinica 18(2):141–151 (in Chinese)

Kalnay E, Kanamitsu M, Kistler R, Collins W, Deaven D, Gandin L, Iredell M, Saha S, White G, Woollen J, Zhu Y, Leetmaa A, Reynolds R, Chelliah M, Ebisuzaki W, Higgins W, Janowiak J, Mo KC, Ropelewski C, Wang J, Jenne R, Joseph D (1996) The NCEP/NCAR 40-year reanalysis project. Bull Am Meteorol Soc 77:431–471

Li C, Ma H (2012) Relationship between ENSO and winter rainfall over southeast China and its decadal variability. Adv Atmos Sci 29(6):1129–1141

Li B, Zhou TJ (2011) ENSO-related principal interannual variability modes of early and late summer rainfall over East Asia in SST-driven AGCM simulations. J Geophys Res 116:D14118. doi:10.1029/2011JD015691

Li H, Dai A, Zhou T (2010a) Responses of East Asian summer monsoon to historical SST and atmospheric forcing during 1950–2000. Clim Dyn 34:501–514. doi:10.1007/s00382-008-0482-7

Li JP, Wu ZW, Jiang ZH, He JH (2010b) Can global warming strengthen the East Asian summer Monsoon? J Clim 23:6696–6705

Liebmann B, Smith CA (1996) Description of a complete (interpolated) outgoing longwave radiation dataset. Bull Am Soc 77:1275–1277

Linderholm HW, Ou T, Jeong J-H, Folland CK, Gong D, Liu H, Liu Y, Chen D (2011) Interannual teleconnections between the summer North Atlantic Oscillation and the summer East Asian Monsoon. J Geophys Res 116:D13107

Madden RA (1976) Estimates of the natural variability of time-averaged sea-level pressure. Mon Weather Rev 104:942–952. doi:10.1175/1520-0493(1976)104<0942:EOTNVO>2.0.CO;2

Mantua NJ, Hare SR, Zhang Y, Wallace JM, Francies RC (1997) A pacific interdecadal climate oscillation with impacts on salmon production. Bull Am Meteorol Soc 78:1069–1079

Mao JY, Chan JCL (2005) Intraseasonal variability of the South China Sea summer monsoon. J Clim 18:2388–2402

Qian C, Zhou T (2014) Multidecadal variability of North China aridity and its relationship to PDO during 1900–2010. J Clim 27(3), 1210–1222, doi:10.1175/JCLI-D-13-00235.1

Quan XW, Diaz HF, Hoerling MP (2004a) Change of the tropical hadley cell since 1950. In: Diaz HF, Bradley RS (eds) Hadley circulation: past, present, and future. Cambridge University Press, New York, pp 85–120

Quan XW, Webster PJ, Moore AM, Chang H-R (2004b) Seasonality in SST forced atmospheric short-term climate predictability. J Clim 17:3090–3180

Rayner NA, Parker DE, Folland CK, Alexander LV, Horton EB, Rowell DP (2003) Globally complete analyses of sea-surface temperature, sea-ice and marine air temperature, 1871–2000. J Geophys Res 108:4407

Song F, Zhou TJ (2014) Interannual Variability of East Asian summer Monsoon simulated by CMIP3 and CMIP5 AGCMs: skill dependence on Indian Ocean-Western Pacific anticyclone teleconnection. J Clim 27:1679–1697

Wang B (2006) The Asian Monson. Springer, Berlin

Wang HJ, He SP (2012) Weakening of relationship between East Asian winter monsoon and ENSO after mid-1970s. Chin Sci Bull 57:3535–3540

Wang B, Li T (2004) East Asian monsoon-ENSO interactions. In: Chang CP (ed) East Asian monsoon. World Scientific, Singapore, pp 177–212

Wang B, Linho (2002) Rainy season of the Asian-Pacific summer Monsoon. J Clim 15:386–398

Wang B, Wu RG, Fu XH (2000) Pacific-East Asian teleconnection: how does ENSO affect East Asian climate? J Clim 13:1517–1536

Wang B et al (2008a) How accurately do coupled climate models predict the leading modes of Asian-Australian monsoon interannual variability? Clim Dyn 30:605–619

Wang B, Yang J, Zhou TJ, Wang B (2008b) Interdecadal changes in the major modes of Asian-Australian Monsoon variability: strengthening relationship with ENSO since late 1970s. J Clim 21:1771–1789

Wang B, Liu J, Yang J, Zhou T, Wu Z (2009) Distinct principal modes of early and late summer rainfall anomalies in East Asia. J Clim 22:3864–3875

Wu RG, Kirtman BP (2007) Observed relationship of spring and summer East Asian rainfall with winter and spring eurasian snow. J Clim 20:1285–1304

Wu T, Qian Z (2003) The relation between the Tibetan winter snow and the Asian summer monsoon and rainfall: an observational investigation. J Clim 16:2038–2051

Wu RG, Wang B (2002) A contrast of the East Asian summer Monsoon-ENSO relationship between 1962–77 and 1978–93. J Clim 15:3266–3279

Wu RG, Hu ZZ, Kirtman BP (2003) Evolution of ENSO-related rainfall anomalies in East Asia. J Clim 16:3742–3758

Wu B, Zhou T, Li T (2009) Seasonally evolving dominant interannual variability modes of East Asian climate. J Clim 22:2992–3005

Wu B, Li T, Zhou TJ (2010) Relative contributions of the Indian Ocean and local SST anomalies to the maintenance of the western North Pacific anomalous anticyclone during El Nino decaying summer. J Clim 23:2974–2986

Wu RG, Yang S, Wen ZP, Huang G, Hu KM (2011) Interdecadal change in the relationship of southern China summer rainfall with tropical Indo-Pacific SST. Theoret Appl Climatol 108:119–133

Xie S-P, Du Y, Huang G, Zheng X-T, Tokinaga H, Hu K, Liu Q (2010) Decadal shift in El Nino influences on Indo-western Pacific and East Asian climate in the 1970s. J Clim 23:3352–3368

Yang J, Liu Q, Xie S-P, Liu Z, Wu L (2007) Impact of the Indian Ocean SST basin mode on the Asian summer monsoon. Geophys Res Lett 34:L02708. doi:10.1029/2006GL028571

Ying KR, Zheng XG, Quan XW, Frederiksen CS (2013) Predictable signals of seasonal precipitation in the Yangtze-Huaihe river valley. Int J Climatol 33:3002–3015. doi:10.1002/joc.3644

Yun K-S, Seo K-H, Ha K-J (2010) Interdecadal change in the relationship between ENSO and the intraseasonal oscillation in East Asia. J Clim 23:3599–3612

Zhang RH, Sumi A, Kimoto M (1999) A diadnostic study of the impact of El Nino on the precipitation in China. Adv Atmos Sci 16:229–241

Zhang YS, Li T, Wang B (2004) Decadal change of the spring snow depth over the Tibetan Plateau: the associated circulation and influence on the East Asian summer Monsoon. J Climate 17:2780–2793

Zhao P, Zhou ZJ, Liu JP (2007) Variability of Tibetan spring snow and its associations with the hemispheric extratropical circulation and East Asian summer Monsoon rainfall: an observational investigation. J Clim 20:3942–3955

Zheng XG, Frederiksen CS (1999) Validating interannual variability in an ensemble of AGCM simulations. J Clim 12:2386–2396. doi:10.1175/1520-0442(1999)012<2386:VIVAE>2.0.CO;2

Zheng XG, Frederiksen CS (2004) Variability of seasonal-mean fields arising from intraseasonal variability: part 1. Methodology. Clim Dyn 23:171–191

Zheng XG, Frederiksen CS (2006) A study of predictable patterns for seasonal forecasting of New Zealand rainfall. J Clim 19:3320–3333. doi:10.1175/JCLI3798.1

Zhou T, Yu R, Li H, Wang B (2008) Ocean forcing to changes in Global monsoon precipitation over the recent half-century. J Clim 21(15):3833–3852

Zhou T, Wu B, Wang B (2009a) How well do atmospheric general circulation models capture the leading modes of the interannual variability of the Asian-Australian Monsoon? J Clim 22:1159–1173

Zhou T, Gong D, Li J, Li B (2009b) Detecting and understanding the multi-decadal variability of the East Asian summer Monsoon—recent progress and state of affairs. Meteorol Z 18(4):455–467

Zhou T, Yu R, Zhang J, Drange H, Cassou C, Deser C, Hodson DLR, Sanchez-Gomez E, Li J, Keenlyside N, Xin X, Okumura Y (2009c) Why the Western Pacific subtropical high has extended westward since the late 1970s. J Clim 22:2199–2215

Zhou LT, Tam CY, Zhou W, Chan CL (2010) Influence of South China Sea SST and the ENSO on winter rainfall over South China. Adv Atmos Sci 27(4):832–844

Zhou T, Hsu H-H, Matsuno J (2011) Summer monsoons in East Asia, Indochina, and the western North Pacific, 43–72 pp. In: Chang C-P et al (eds) The Global Monsoon system: research and forecast (2nd edn). World Scientific Publishing Co, Singapore

Zhou T, Song F, Lin R, Chen X, Chen X (2013) The 2012 North China floods: explaining an extreme rainfall event in the context of a long-term drying tendency [in "Explaining Extreme Events of 2012 from a Climate Perspective"]. Bull Am Meteorol Soc 94(9):S49–S51

Zuo JQ, Li WJ, Sun CH, Xu L, Ren HL (2013) Impact of the North Atlantic Sea surface temperature Tripole on the East Asian summer Monsoon. Adv Atmos Sci 30(4):1173–1186